Conf-901105--69

CONF-901105--69

DE91 006421

NEUTRON TOMOGRAPHY: A SURVEY AND SOME RECENT APPLICATIONS*

E. A. Rhodes[1], J. A. Morman[1], and G. C. McClellan[2]

[1]Reactor Engineering Division
Argonne National Laboratory
Argonne, Illinois 60439

[2]Argonne West
P.O. Box 2528, Idaho Falls, Idaho 83403

Paper submitted for the Materials Research Society
1990 Fall Meeting
Boston, Massachusetts
November 26—December 1, 1990

*Work supported by the U.S. Department of Energy, Office of Technology Support

NEUTRON TOMOGRAPHY: A SURVEY AND SOME RECENT APPLICATIONS

E. A. RHODES*, J. A. MORMAN*, AND G. C. McCLELLAN**
*Argonne National Laboratory, 9700 S. Cass Ave., Argonne, IL 60439
**Argonne-West, P. O. Box 2528, Idaho Falls, ID 83403-2528

ABSTRACT

A survey is given of recent developments in selected areas of neutron tomography, within the context of several applications Argonne is involved in, including high penetration of reactor-fuel bundles in thick containers (involving TREAT and NRAD facilities), dual-energy hydrogen imaging (performed at IPNS), dynamic coarse-resolution emission tomography of reactor fuel under test (a proposed modification to the TREAT hodoscope), and an associated-particle system that uses neutron flight-time to electronically collimate transmitted neutrons and to tomographically image nuclides identified by reaction gamma-rays.

INTRODUCTION

Unlike gamma-rays, neutrons transmitted through materials react with nuclei rather than electrons. Neutrons can deeply penetrate many materials (allowing tomographic radiography of thick objects), neutron transmission cross-sections often vary strongly with energy and nuclide (yielding "fingerprints" for various nuclides), and neutron reactions often occur that produce gamma-rays having distinct spectra (giving wide-range identification of specific nuclides). Neutrons provide a uniquely useful diagnostic probe for characterization of materials, and examples are given that illustrate these properties.

Traditionally neutron tomography is performed at a reactor using film measurements of thermal-neutron transmission at many orientations, followed by microdensitometer film scans and computer reconstruction from projections. However many aspects of neutron tomography are changing. Within the context of some applications Argonne is involved in, a survey is given of related recent developments in source, detection, data acquisition, and computer reconstruction technologies that are making neutron tomography more accessible, in the sense of new applications, less expensive and more transportable equipment, and faster measurements. The Argonne applications focus on penetration of thick objects and comprehensive materials identification. Minimization of measurement times is more important than high spatial resolution in most of the applications discussed, and medium to low (mm to cm) spatial resolution is adequate in most cases.

EPITHERMAL RADIOGRAPHY OF REACTOR FUEL

At the TREAT (Transient Reactor Test facility) reactor at Argonne-West, prototypic reactor fuel assemblies heated by fission inside capsules or coolant loops are driven to destruction by transient overpower and/or coolant flow coastdown conditions designed to simulate HCDAs (Hypothetical Core Disruptive Accidents). During the actual test, a fast-neutron hodoscope dynamically records a 2D image of the fuel as it melts and relocates [1]. For analysis of HCDA progressions and consequences, it is also important to examine the final distribution of fuel, clad, and coolant and determine metallurgical material changes. The standard technique for this is laborious remote post-test destructive examination of the irradiated assembly at HFEF (Hot Fuel Examination Facility) at Argonne-West, where transverse sections are cut, polished, and studied macroscopically and microscopically.

Neutron tomography is now being developed to complement post-test destructive examinations, by providing a guide to locate optimal sectioning positions and to reduce the number of section cuts necessary, as well as by yielding many more transverse section images than possible with destructive sectioning. The goal is to provide more comprehensive and quantitative post-test material distributions. The test fuel has a high gamma-ray radiation level and would fog direct X-ray or neutron-sensitive films, so the indirect process of neutron activation of foils is used, with subsequent activity transfer to film. The high-density test fuel strongly absorbs thermal neutrons. Also, in order to preserve the distribution of materials, in some cases the test fuel needs to be radiographed prior to disassembly from an outer container ~ 15 mm thick. Thus epithermal neutron radiography is required.

The neutron radiographs are produced at the north beam tube of the NRAD 250-kW TRIGA reactor at HFEF [2]. The tube extends from the core face to obtain a relatively hard spectrum containing many epithermal neutrons. L/D ratios of 185, 300, and 700 are available, for radiographs up to 43 cm x 36 cm in size. The radiographing process is illustrated in Fig. 1. A fuel-pin bundle is suspended on a precision rotator for the many views required. At each view a packet of foils is irradiated for 30-60 min., a cadmium foil in front to attenuate thermal neutrons and an indium imaging foil to capture epithermal neutrons at the 1.45 eV indium resonance. The indium foils are removed and placed in contact with photographic film (usually type T). After the decaying indium exposes the films, they are developed and then digitized on a scanning microdensitometer.

A computer program aligns each view image and calibrates the density from a step wedge image in each view. Then a computed tomography transverse cross-section is reconstructed for each desired elevation. As an illustration of the penetration and imaging capability of indium resonance tomography, Fig. 2 shows a reconstructed cross-section of a 91-pin EBR-II fuel bundle using only 36 views [3]. Each pin is U metal 3.68 mm in diameter. Spiral spacer wires are also evident. The image has been high-pass filtered and clipped.

Shown in Fig. 3 are a series of transverse reconstructions of the remains of an assembly containing seven mixed Pu-U oxide fuel pins after TREAT test LO7, compared to cut and polished sections at the same elevations [4]. Seventy-six views were used and the densitometer aperture was set at 0.1 mm horizontally and 0.2 mm vertically. Intact fuel pins are 5.84 mm in diameter and are supported by grid spacers. Unfortunately the transverse reconstructions in Fig. 3 are from pseudocolor images and cannot be compared easily in density to the cut sections, for which steel is light and fuel and voids are dark, but the spatial details are similar (in some cases material present during radiography has been lost during destructive examination). Not shown are useful axial reconstructions obtained by stacking the transverse reconstructions and slicing through them computationally.

At the present stage of development, the reconstructions identify relocated fuel and steel, flow tube blockages, and pin displacement, but do not reliably distinguish between fuel and steel in very irregular geometries and provide little information on cladding condition. To go further into quantitative analysis of materials distributions and to separate boundary features of hex cans, grid spacers, fuel pins, and cladding, improved spatial and density resolution are required. This will necessitate higher resolution film digitization, which will increase the already long 3 films/day microdensitometer scanning times. However modern digitizers are available that can scan a radiograph in 30 s with sufficient spatial and density resolution, and there are plans to buy one. Possibly many more that the present 76 views will be needed, leading to much longer reactor operation. Around an hour will be required for each radiograph, due to low indium foil activation, and two to five radiographs will be needed for each view to cover the test-fuel length.

Perhaps a tomographic algorithm can be found that will provide good reconstructions with fewer views, minimizing reactor time. The currently used

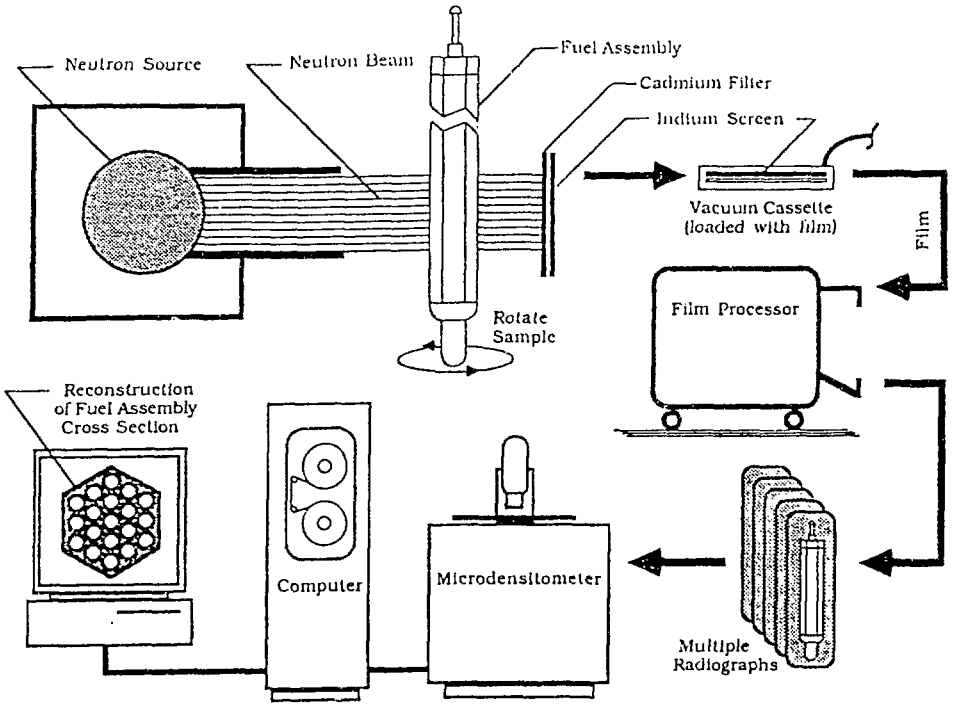

Fig. 1. NRAD indium-resonance neutron radiography process.

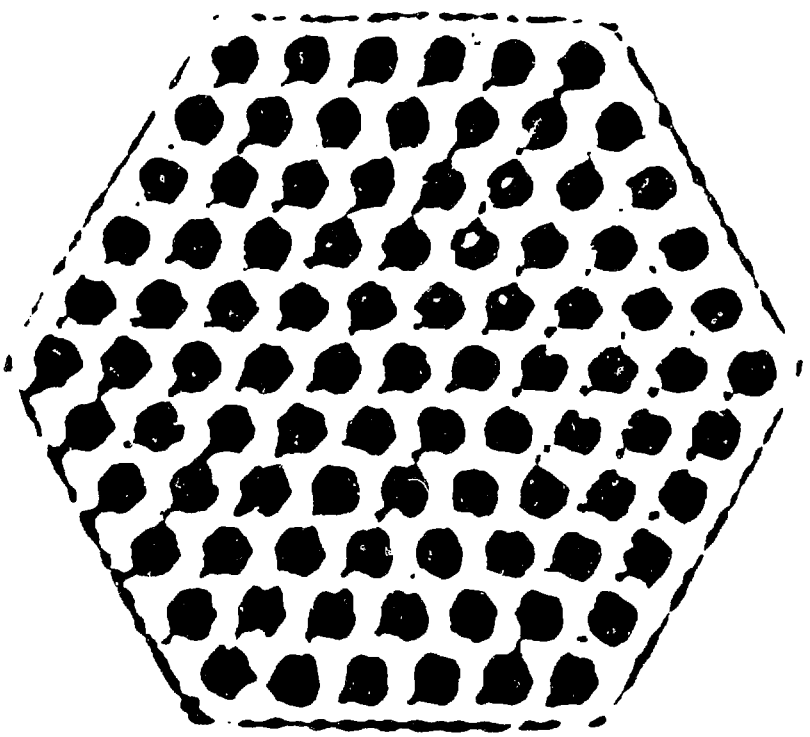

Fig. 2. NRAD reconstruction of an EBR-II 91-pin fuel bundle.

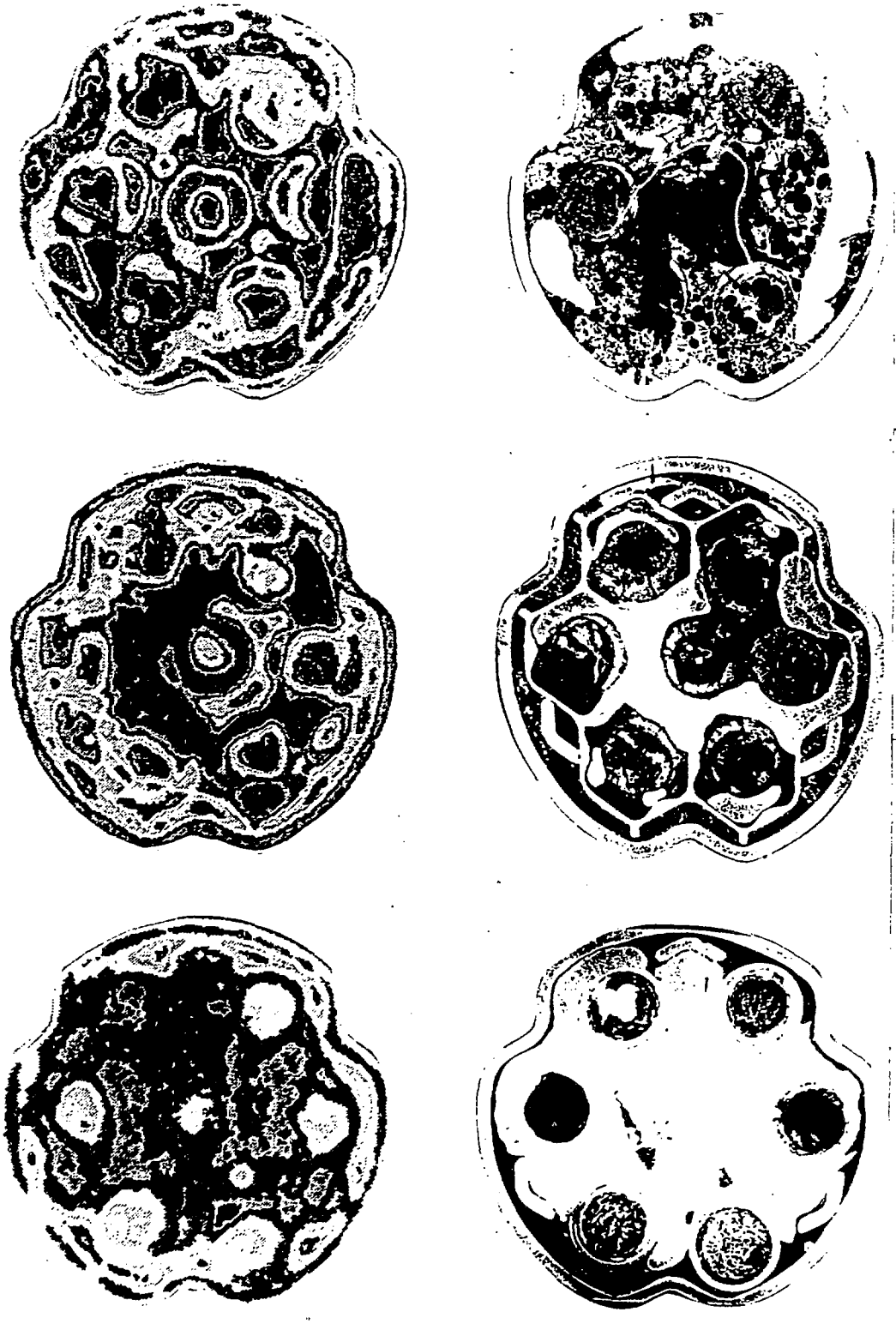

Fig. 3. Comparison of LO7 transverse reconstructions (left) with cut sections (right) at elevations of 97 mm (top), 71 mm (center), and -3 mm (bottom).

filtered backprojection allows quick calculation but requires trial-and-error filter optimization. Other linear algorithms are available that implement gradient, convolution, minimum variance, and regularization methods, among others [5,6]. Nonlinear tomographic methods that provide positive-definite image constraints, such as MART [6], maximum entropy [7], and maximum likelihood (EM) [8], may hold more promise for use of fewer views. Figure 2 was reconstructed from only 36 views using a maximum entropy algorithm. The nonlinear methods are less susceptible to noise and are less prone to image artifacts, but require intensive iterative computations. Such computations pose little problem for modern high-speed computers, but it remains to be seen how accurately nonlinear reconstruction algorithms preserve spatial and density resolution in asymmetric geometries.

MULTIPLE-ENERGY NEUTRON TOMOGRAPHY

In multiple-energy neutron tomography, specific nuclides are imaged or their images are enhanced by using the differences in cross-section variation with neutron energy of the nuclides present, by either subtracting tomographic images or by producing several different sets of radiographs at different neutron energies, often by simultaneously distinguishing different neutron energies during one exposure. Use of a pulsed accelerator and active neutron detectors time-gated to the beam allows simultaneous selection of desired neutron energies by flight-time measurement. In this manner, resonance radiography has been performed at the NIST electron linac from 1 to 40 eV [9] and at the Argonne IPNS (Intense Pulsed Neutron Source) from 0.3 to 10 eV [10], in which separate images are formed at discrete resonance energies where there are strong increases in neutron absorption for nuclides of interest (actinides, rare earths, and fission products for $Z > 40$, at these energies). Images of each nuclide are unfolded from the resonance patterns.

Another technique is dual-energy hydrogen imaging, in which the increase in hydrogen neutron cross-section at subthermal neutron energies is used to enhance the imaging of small amounts of hydrogen against a background of other absorbing materials by subtracting a tomographic image obtained for higher energy neutrons from that obtained for subthermal neutrons (picking energies such that the other absorbing materials have nearly the same cross-sections at both energies). This technique was used to provide dual-energy imaging of water in tuffaceous rock [11], with the goal being to track water flow through porous rock for site risk analysis of permanent disposal of radwaste. A feasibility experiment was conducted at the IPNS facility with coarse spatial resolution, collecting neutrons at 15 and 85 meV in a scanned ^{3}He detector. The setup is shown in Fig. 4. At IPNS, 30 intense pulses of 500 MeV protons per second strike a U target, where spallation produces fast neutrons that are moderated to low energies. Neutron energies are simultaneously selected by measuring moderator flight time.

Measurements were taken at four scan positions for three views of a tuff sample sketched in Fig. 5. The crack shown contained water, particularly at the outer rim. Coarse-resolution reconstructions were performed using the convolution algorithm. The image obtained by subtracting the reconstruction at 85 meV from that at 15 meV is shown in Fig. 6. The darker regions indicate the strongest absorption and are consistent with expected presence of water (the sample in Fig. 6 is rotated from the sketch in Fig. 5). Absorption differences due to rock boundaries, ie. the sample rim and the crack (except for water), are nearly invisible, so that a clean enhanced image of water is obtained.

SOME RECENT HARDWARE DEVELOPMENTS

Recent hardware developments have led to progress in some areas of neutron tomography. In the past few years, relatively high resolution active 2D detectors have been developed that are efficient for thermal and epithermal neutrons. Wide-

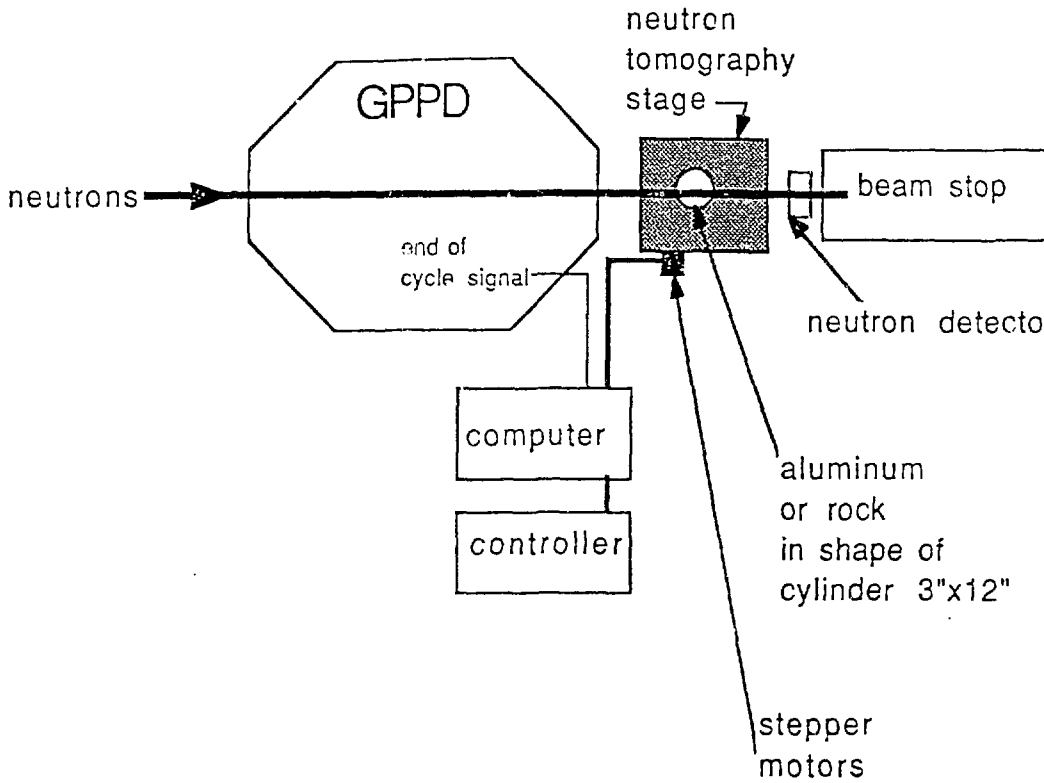

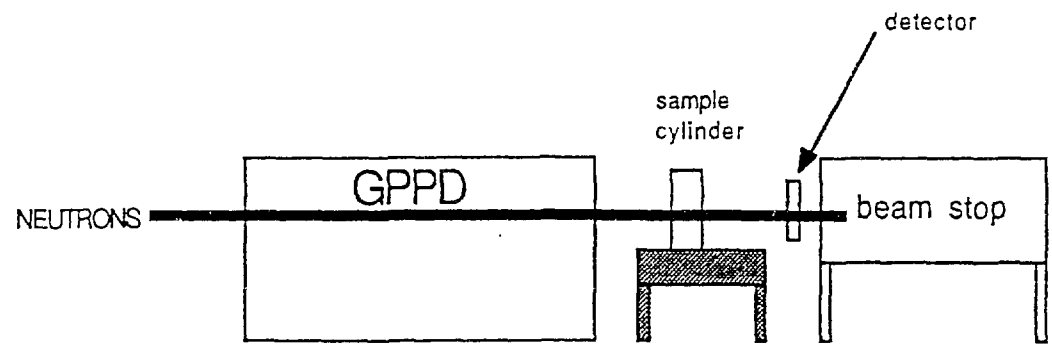

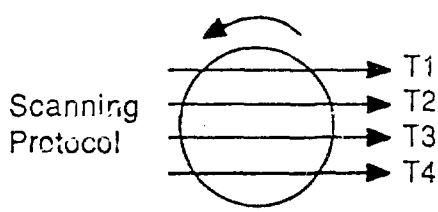

N-Beam Along Line	Rotational Position (deg)
T1	0, 120, 240
T2	0, 120, 240
T3	0, 120, 240
T4	0, 120, 240

Fig. 4. IPNS setup for dual-energy imaging of water in tuff.

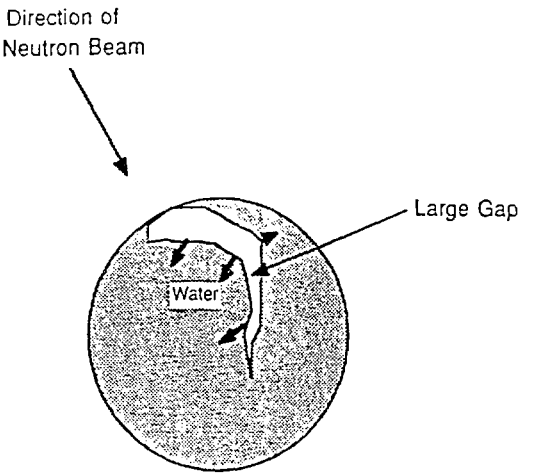

Fig. 5. Approximate sketch of tuff cross-section.

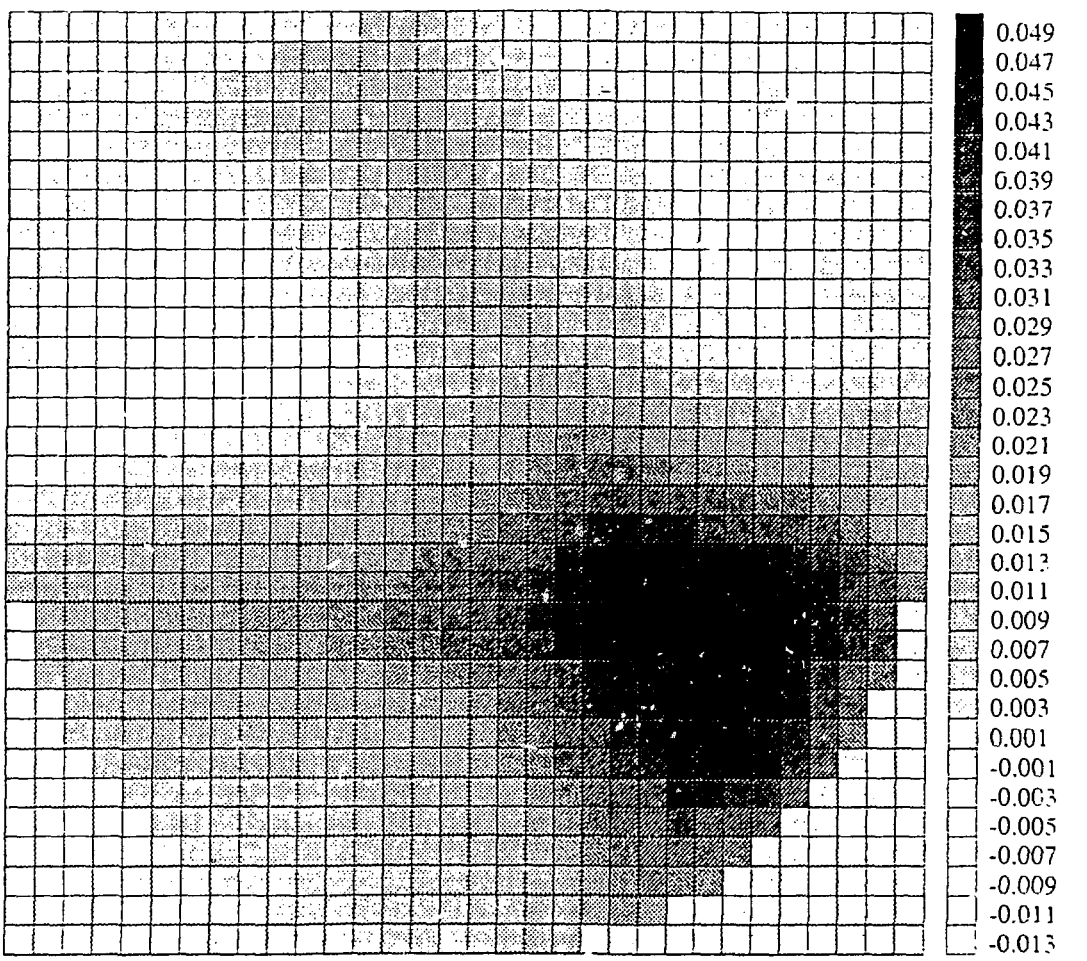

Fig. 6. Subtractive dual-energy reconstruction of tuff cross-section (rotated from sketch in Fig. 5).

area detectors include a 5 cm x 5 cm crossed-wire proportional counter of 1-mm resolution containing a high-pressure gas mixture [12], and a 22-cm diameter neutron Anger camera of 2-mm resolution, based on a glass scintillator optically coupled by a light guide to 19 close-packed photomultipliers [13].

The most prevalent detectors use a 2D image intensifier of some type, the simplest being a ZnS (or other) converter screen of arbitrary size viewed through a lens by a low-light-level TV camera containing an intensifier [14]. One image intensifier tube has a 23-cm diameter Gd_2O_2S converter screen and electrodes that focus the electrons onto a scintillation screen that is viewed by a TV camera [15]. A third type of intensified detector is a Lixiscope fronted by a 5-cm diameter neutron-sensitive scintillator, with fibre optics, a photocathode, and a microchannel plate. The output can be either a phosphor screen for TV camera viewing [16] or a resistive anode for electronic interfacing [12]. Intensified detectors are capable of resolutions from around 50 to 500 microns, depending on detection area.

The availability of these detectors has aided development of new neutron radiography applications. Dynamic 2D radiography has become possible for large (reactor) and medium (accelerator) neutron sources, with applications in fluid flow [17] and mechanical motion [18]; although the images tend to be somewhat noisy and resolution and contrast are substantially lower than attainable in static neutron radiography, useful motion is observed. For small (^{252}Cf and deuteron-on-tritium, or D/T, generator) neutron sources, transportable 2D radiography systems have been built for applications such as aircraft inspection [19]. Intense transportable sources are being developed, including a high-output D/T generator [20] and accelerators based on bombardment of Be by protons or deuterons, such as a superconducting cyclotron [21] and small rf linacs [22].

These neutron detector and source developments lead one to contemplate the potential for dynamic 3D neutron tomography. Key features of any system capable of this would be the use of efficient 2D detectors, the attainment of 2D and depth resolution simultaneously, and stationary sources and detectors. Coded apertures (for emission, or auto-radiography), such as any of a number of arrangements of multiple pinholes or a Fresnel zone plate, and corresponding coded sources (for transmission radiography) come to mind, since they cast shadows on the detectors that vary in size with distance of objects from the detector and that can be decoded to yield depth information. However they have not been successful for neutron radiography when a substantial number of voxels is desired in the 3D image, because of neutron penetration of and scattering in the structure of the coded aperture or source and resulting image artifacts.

Another possibility might be a stereoscopic pair of sources and detectors. Although this would allow determination of the order in depth of well-separated objects, little detailed depth resolution would result. The use of simultaneous views around the object to be radiographed, with a source/detector combination for each view, would be more likely to provide successful dynamic 3D tomography, but much hardware would be involved unless a small number of views will yield adequate 3D resolution. As an example of a system for dynamic 3D neutron tomography, a proposed system based on an intense source and massively parallel detectors will be discussed, a tomographic fast-neutron hodoscope, that is based on the present 2D TREAT hodoscope mentioned earlier.

Elevation and plan views of the present TREAT hodoscope [1] are shown in Fig. 7. It provides dynamic 2D emission radiography by detecting fission neutrons emitted by test fuel in a capsule or loop at the center of the TREAT reactor core, using time-resolved readouts of a 2D detector array. Test fuel is driven to destruction during a reactor transient, in order to simulate an HCDA, and the hodoscope captures the resulting fuel motion for later analysis. The test fuel is viewed through a large steel collimator, which contains 360 channels, 36 rows x 10 columns. Fast-neutron detectors are located behind each channel, and all detectors

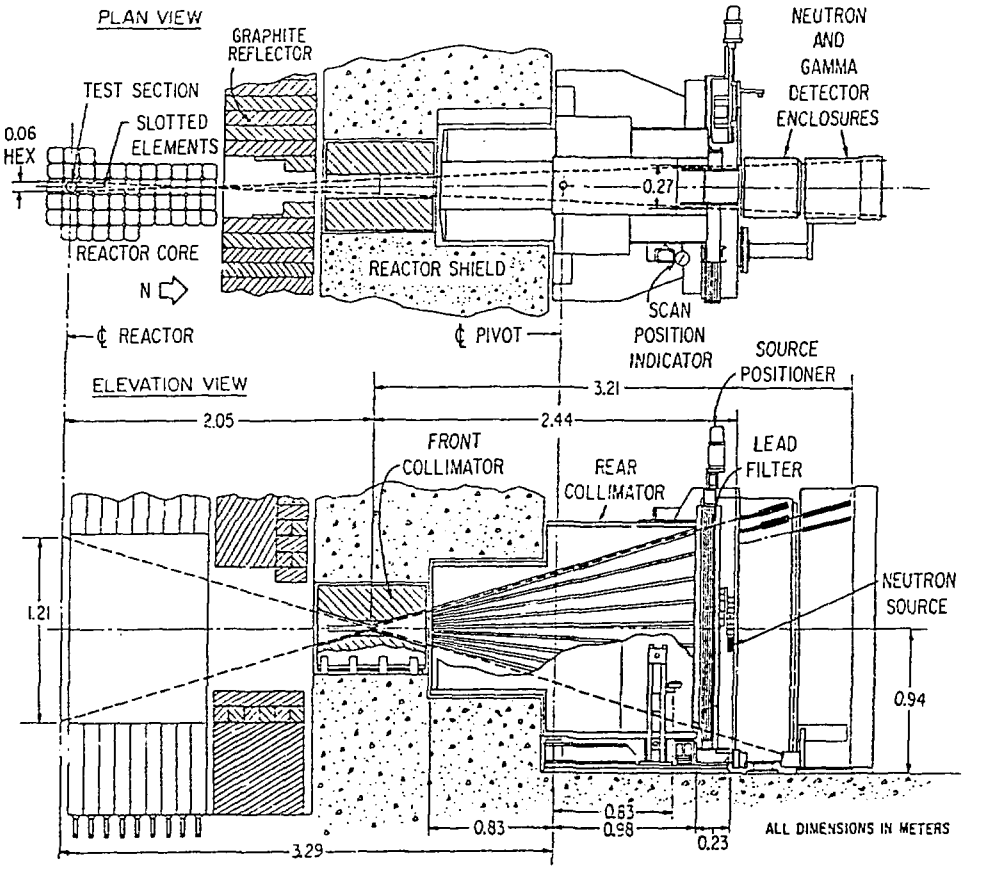

Fig. 7. Diagram of TREAT fast-neutron hodoscope.

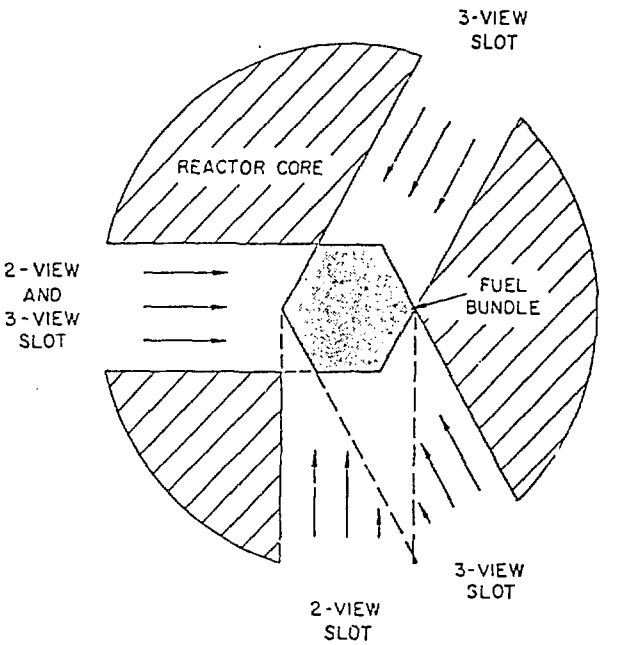

Fig. 8. Plan view of hodoscope arrangements for tomographic resolution in STF.

read out in parallel to a computer data acquisition system. This system emphasizes time resolution, rather than spatial resolution, as required by the experiments: the data collection interval is 0.3 ms to several ms and interchannel spacing at the test plane is 6.6 mm horizontally and 34.5 mm vertically.

There was a desire to provide depth resolution for proposed future STF tests of large fuel bundles. The possible arrangements proposed to perform dynamic 3D neutron tomography, two 2D hodoscopes at 90 deg. or three at 120 deg., are illustrated in Fig. 8. It was found in a study of computer-generated phantoms and reconstructions [23] that a substantial amount of tomographic resolution could be attained using specialized reconstruction methods for 2 and 3 views.

ASSOCIATED-PARTICLE TOMOGRAPHY

Recently Argonne has been involved with the associated-particle tomography method, a potentially powerful diagnostic tool. In this method, a special D/T generator containing an alpha-particle detector irradiates the object of interest with 14-MeV neutrons. As shown in the schematic layout in Fig. 9, deuterons are accelerated into a tritium target, producing 14-MeV neutrons isotropically. Each neutron is accompanied by an associated alpha-particle going in the opposite direction. The gamma-ray and neutron detectors are time-gated by pulses from the alpha detector, which forms a cone of flight-time-correlated neutrons through the object. When a reaction occurs in the object along the cone that results in a detected gamma-ray, the time-delay from the alpha pulse yields the position (depth) along the cone where the reaction occurred, since the source neutron and gamma-ray speeds are known. By scanning the alpha detector horizontally and vertically (or by using a 2D multipixel alpha detector), 2D plus depth locations of reaction sites can be mapped, providing 3D emission imaging of reaction densities.

Energy spectra of the gamma detectors are recorded. Fast-neutron (prompt) inelastic scattering reactions in the object provide spectra that can identify many nuclides. By choosing gamma lines of specific nuclides, a 3D image of each identifiable nuclide can be mapped. By choosing appropriate nuclide intensity ratios, 3D images of compounds can be made. Slow-neutron capture is not prompt and thus not time-correlated with the alpha pulses, but provides nonimaging spectra that can aid nuclide identification. By discarding detected neutrons not having the proper flight time to be uncollided, one can perform fast-neutron 2D transmission imaging without a collimator (by scanning or using 2D neutron detectors), since scattered neutrons are removed by "electronic collimation". By measuring at a sufficient number of views around 180 deg., 3D tomography is feasible. Transmission imaging can be done along with or instead of emissive reaction-density imaging.

In the actual system, a PC controls the experiment, collects the flight-time and energy data, calculates positions, and displays data and images. The heart of the system is the state-of-the-art APSTNG (Associated-Particle Sealed-Tube Neutron Generator) developed with considerable effort by C. Peters, manager of the Advanced Systems Division of Nuclear Diagnostic Systems Inc. As diagrammed in Fig. 10, a Penning ion source emits a mixed beam of deuterium and tritium ions that is accelerated and focused on a small spot on the target, tritiating the target and producing neutrons and alpha particles. The alpha detector consists of a ZnS screen and a photomultiplier. The APSTNG is a relatively inexpensive small sealed module with low-bulk support equipment. It has a long MTBF (exceeding 2000 hours at a million n/s or 200 hours at 10 million n/s), is easily replaced by a remanufactured module, and presents low radiation exposure.

A proof-of-principle experiment on gamma-ray emission reaction-density imaging was performed on an interrogation volume containing a carbon block and an aluminum block and plate. Shown in Fig. 11 are the gamma-ray energy spectra

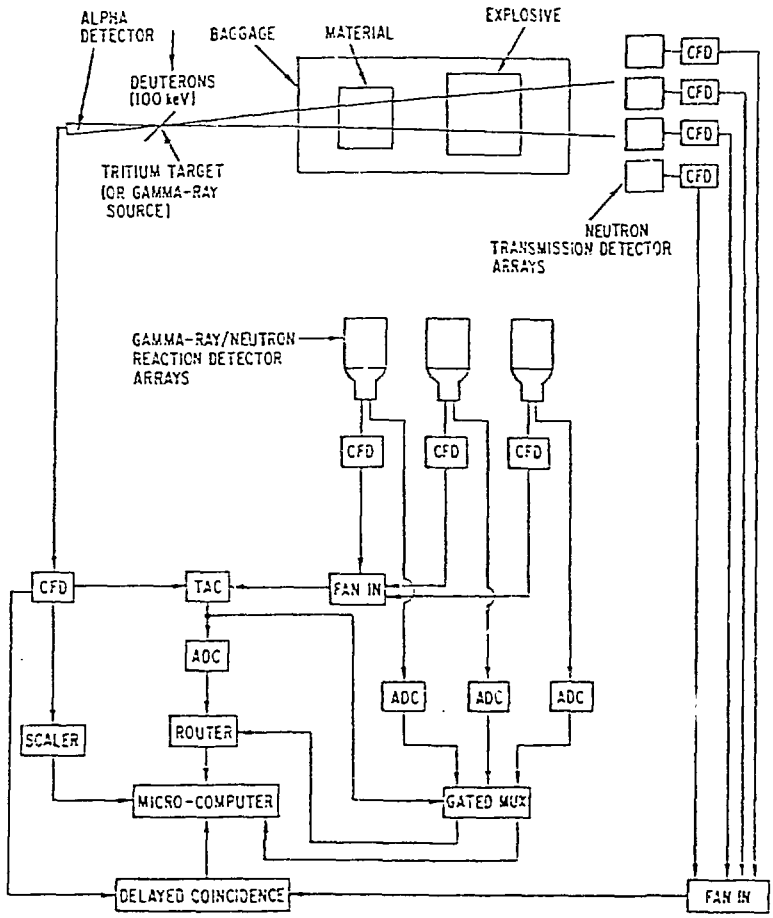

Fig. 9. Schematic layout of associated-particle interrogation system.

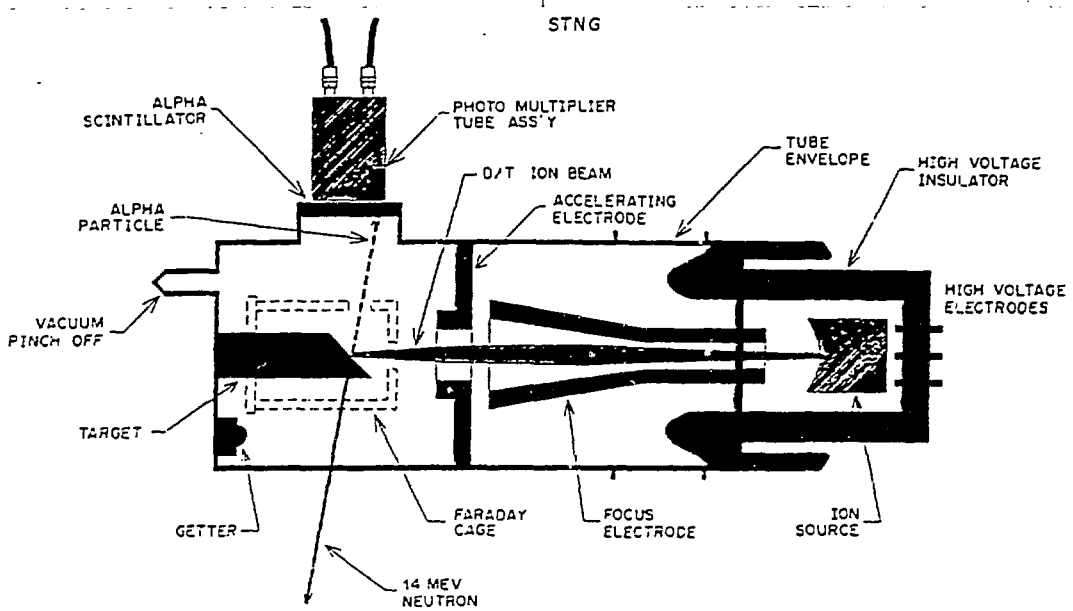

Fig. 10. Diagram of APSTNG (Associated-Particle Sealed-Tube Neutron Generator).

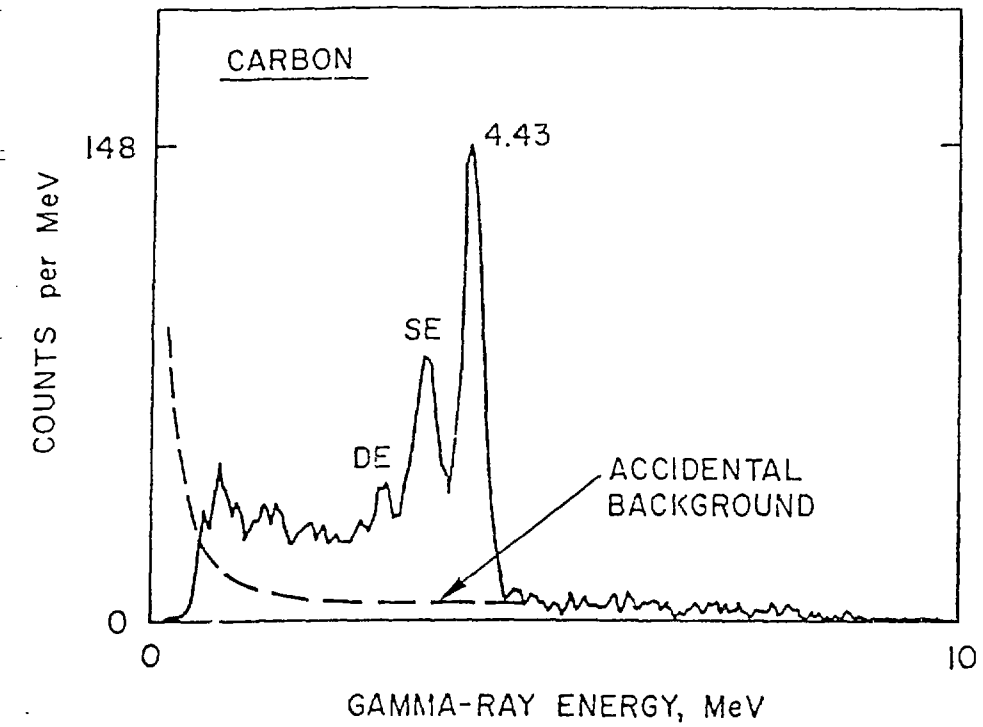

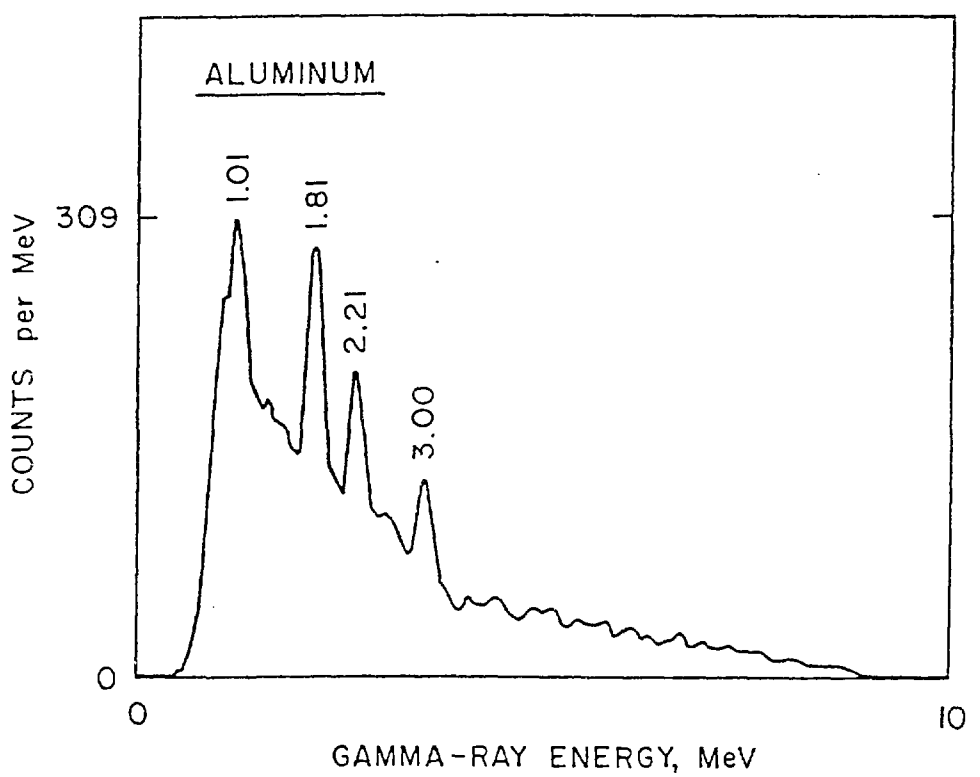

Fig. 11. APSTNG system gamma-ray energy spectra of C and Al targets.

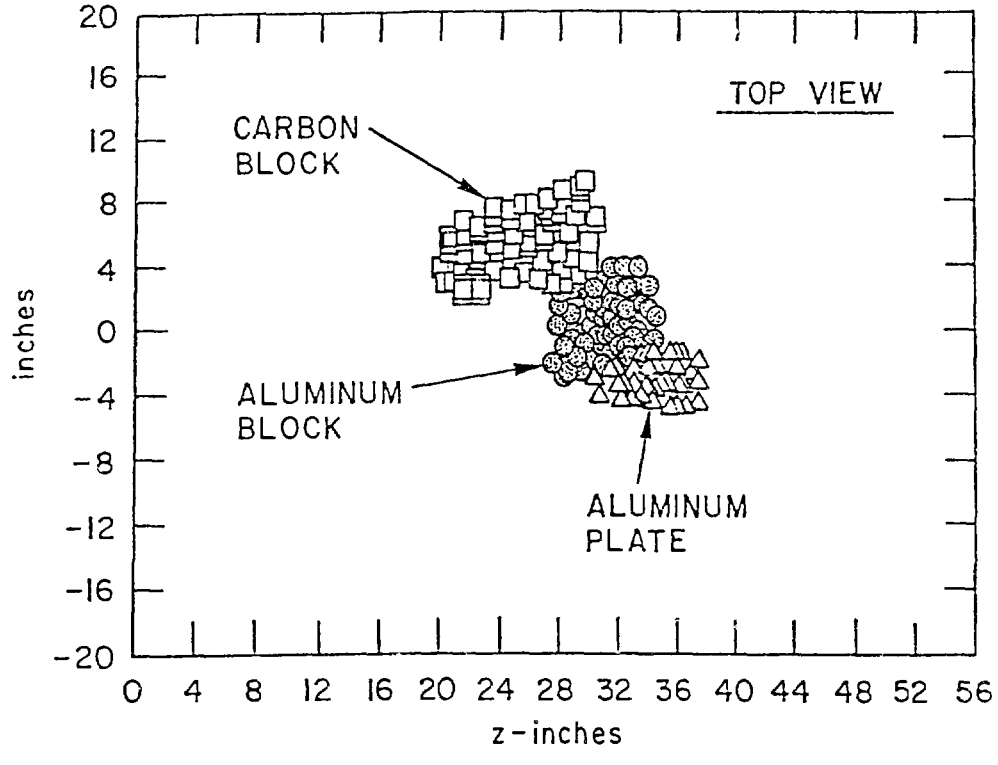

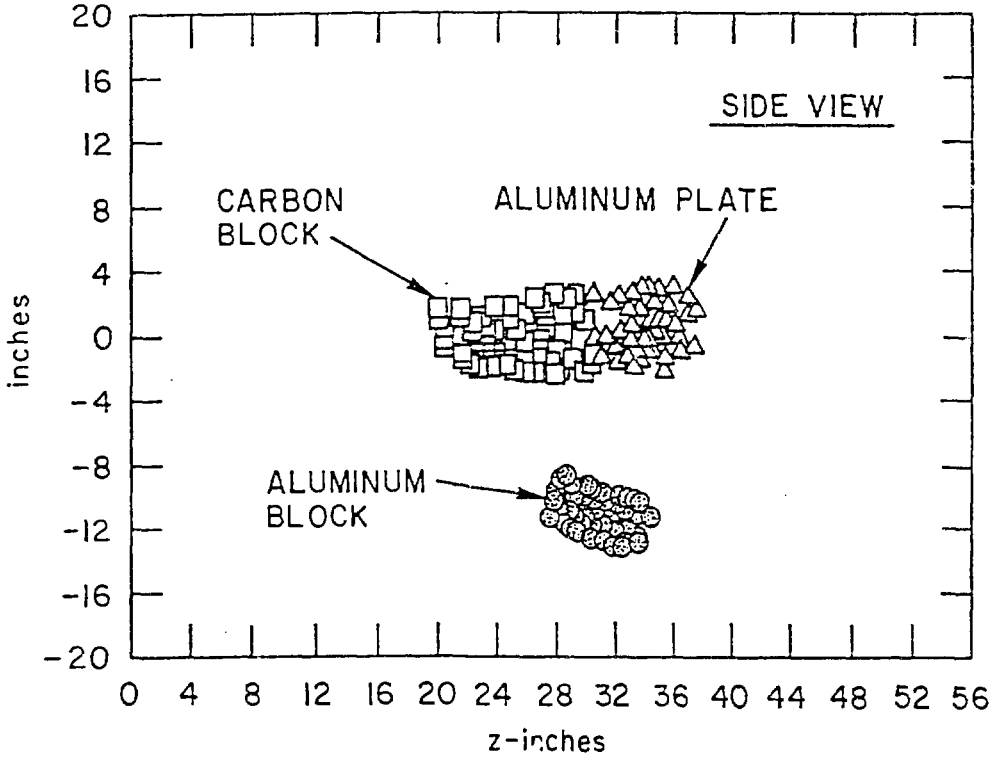

Fig. 12. Top and side views of 3D location of C and Al targets as mapped from APSTNG gamma-ray emission data. Points indicate mapped reaction sites.

for neutron inelastic scattering obtained for C and Al. By scanning a single-pixel alpha detector over one side of the volume (x and y coordinates) and mapping reaction sites from flight-time along the correlation cone (z coordinate) for energy windows enclosing C and Al gamma lines, the objects were correctly identified and 3D-imaged, as shown in Fig. 12. Proof-of-concept experiments have been successfully done for a number of applications: chemical ordnance identification explosive detection and identification, contraband drug detection, uranium borehole logging, corrodent detection on turbine blades, kerogen analysis of shale, and contents of coals (sulfur, minerals, and btu).

APSTNG technology has the capabilities for identification and 3D imaging of many individual nuclides and compounds, with flexible positioning of reaction detectors with respect to the neutron source (on the same side, perpendicular, or opposite side), as well as capability for fast-neutron transmission imaging. The source and emitted radiation are high-energy and allow penetration of highly absorbing objects. But there are some limitations that can be significant in certain applications of this technology. With regard to transmission imaging, development of a 2D fast-neutron detector having sufficient efficiency will involve resolution tradeoff. With regard to emissive reaction-density imaging, images will be significantly attenuated with depth into the interrogated object if it is strongly absorbing, presently attainable depth resolution is limited to 5 cm (because the system has an overall time resolution of ~ 1 ns and a 14-MeV neutron travels 5 cm in 1 ns), and measurement times can be rather long to obtain sufficient gamma counts.

The gamma signal count rate is limited by reaction cross-sections, solid angles subtended by the alpha detector and gamma detectors, gamma detector efficiency, and source strength, but source strength is limited by detector accidental counts and pileup. The use of a relatively large array of small gamma detectors or a relatively small array of large flight-time sensitive gamma detectors is being investigated for increasing the count rate while maintaining depth resolution for emissive imaging. The fabrication of a relatively large 2D alpha detector is also being considered, for increasing the signal rate while maintaining transverse resolution.

REFERENCES

1. A. DeVolpi, C. L. Fink, G. E. Marsh, E. A. Rhodes, and G. S. Stanford, Nucl. Tech. **56**, 141 (1982).

2. W. J. Richards, G. C. McClellan, and D. M. Tow, Matl. Eval. **40**, 1263 (1982).

3. D. M. Tow, Neutron Radiography: Proceedings of the First World Conference (San Diego, CA, Dec. 7-10, 1981), 425.

4. J. A. Morman, P. H. Froehle, J. W. Holland, and J. D. Bennett, Proceedings of the 1990 International Fast Reactor Safety Meeting (Snowbird, UT, Aug. 12-16, 1990) I, 441.

5. R. H. Huesman, G. T. Gullberg, W. L. Greenburg, and T. F. Budinger, Users Manual: Donner Algorithms for Reconstruction Tomography, Pub. 214, Lawrence Berkeley Laboratory, Univ. of California, Berkeley CA, (Oct. 1977).

6. G. T. Herman, R. M. Lewitt, Dewey Odhner, and S. W. Rowland, SNARK89: A Programming System for Image Reconstruction from Projections, Medical Image Processing Group Tech. Rpt. No. MIPG160, Dept. of Radiology, Univ. of Pennsylvania, Philadelphia, PA (Nov. 1989).

7. G. Minerbo, Comput. Biol. Med. **9**, 29 (1979).

8. K. Lange and R. Carson, J. of Computer Assisted Tomography **8**, 306 (1984).

9. C. D. Bowman, R. A. Schrack, J. W. Behrens, and R. G. Johnson, *ibid* Ref. 3, 503.

10. M. G. Strauss, G. H. Lander, R. Brenner, and C. T. Roche, *ibid* Ref. 3, 519.

11. D. S. Kupperman, R. L. Hitterman, and E. Rhodes, Proceedings of the 17th Annual Review of Progress in Quantitative NDE (San Diego, CA, July 1990).

12. R. A. Schrack *et al*, *ibid* Ref. 3, 495.

13. M. G. Strauss, R. Brenner, F. J. Lynch, and C. B. Morgan, IEEE Trans. Nucl. Sci. **NS-28** (1), 800 (Feb. 1981).

14. W. E. Dance and S. F. Carollo, Neutron Radiography: Proceedings of the Second World Conference (Paris, France, June 16-20, 1986), 415.

15. Vijay Alreja and Leonard Corso, *ibid* Ref. 14, 625.

16. J. T. Lindsay, J. D. Jones, C. W. Kaufman, and B. Van Pelt, Nucl. Instr. **A242**, 525 (1986).

17. John M. Cimbala, Dhushy Sathianathan, Stephen A. Cosgrove, and Samuel H. Levine, Neutron Radiography: Proceedings of the Third World Conference (Osaka, Japan, May 14-18, 1989), 497.

18. Koichi Sonoda, Atsuo Ono, Eiichi Hiraoka, Ryoichi Taniguchi, Shuichi Tazawa, and Takehiko Nakanii, *ibid* Ref. 17, 539.

19. V. J. Orphan, T. Maung, and R. Polichar, *ibid* Ref. 17, 749.

20. Serge Cluzeau and Michel Dubouchet, *ibid* Ref. 17, 205.

21. M. R. Hawkesworth, *ibid* Ref. 14, 183.

22. Robert W. Hamm, *ibid* Ref. 17, 231.

23. A. DeVolpi and E. A. Rhodes, Matl. Eval. **40**, 1273 (1982).